



# Aggrecan accumulates at sites of increased pulmonary arterial pressure in idiopathic pulmonary arterial hypertension

Oscar van der Have<sup>1</sup>  | Timothy J. Mead<sup>2</sup>  | Christian Westöö<sup>1</sup> |  
 Niccolò Peruzzi<sup>1,3</sup> | Ayse C. Mutgan<sup>4,5</sup> | Christian Norvik<sup>1</sup> | Martin Bech<sup>3</sup> |  
 André Struglics<sup>6</sup> | Konrad Hoetzenecker<sup>7</sup> | Hans Brunnström<sup>8,9</sup> |  
 Gunilla Westergren-Thorsson<sup>1,10</sup> | Grazyna Kwapiszewska<sup>4,5,11</sup> |  
 Suneel S. Apte<sup>2</sup> | Karin Tran-Lundmark<sup>1,10,12</sup>

<sup>1</sup>Department of Experimental Medical Science, Faculty of Medicine, Lund University, Lund, Sweden

<sup>2</sup>Department of Biomedical Engineering, Cleveland Clinic Lerner Research Institute, Cleveland, Ohio, USA

<sup>3</sup>Department of Medical Radiation Physics, Clinical Sciences Lund, Lund University, Lund, Sweden

<sup>4</sup>Ludwig Boltzmann Institute for Lung Vascular Research, Graz, Austria

<sup>5</sup>Division of Physiology, Otto Loewi Research Center, Medical University Graz, Graz, Austria

<sup>6</sup>Department of Clinical Sciences Lund, Orthopaedics, Faculty of Medicine, Lund University, Lund, Sweden

<sup>7</sup>Department of Thoracic Surgery, Medical University of Vienna, Vienna, Austria

<sup>8</sup>Department of Clinical Sciences Lund, Division of Pathology, Faculty of Medicine, Lund University, Lund, Sweden

<sup>9</sup>Department of Genetics and Pathology, Division of Laboratory Medicine, Lund, Sweden

<sup>10</sup>Wallenberg Center for Molecular Medicine, Lund University, Lund, Sweden

<sup>11</sup>Institute for Lung Health, Justus Liebig University, Giessen, Germany

<sup>12</sup>The Pediatric Heart Center, Skåne University Hospital, Lund, Sweden

## Correspondence

Oscar van der Have, Sölvegatan 19, BMC C12, Vessel Wall Biology, 22184 Lund, Sweden.

Email: [oscar.van\\_der\\_have@med.lu.se](mailto:oscar.van_der_have@med.lu.se)

## Funding information

The Skåne County Council; The Royal Physiographic Society of Lund; Crafoordska Stiftelsen; NIH Clinical Center, Grant/Award Number: HL141130; The Knut and Alice Wallenberg foundation; The Swedish Heart-Lung Foundation, Grant/Award Number: 20220591; The Swedish Society of Medicine; The Lund Society of Medicine; The Swedish Research Council, Grant/Award Number: 2022-00683

## Abstract

Expansion of extracellular matrix occurs in all stages of pulmonary angiopathy associated with pulmonary arterial hypertension (PAH). In systemic arteries, dysregulation and accumulation of the large chondroitin-sulfate proteoglycan aggrecan is associated with swelling and disruption of vessel wall homeostasis. Whether aggrecan is present in pulmonary arteries, and its potential roles in PAH, has not been thoroughly investigated. Here, lung tissue from 11 patients with idiopathic PAH was imaged using synchrotron radiation phase-contrast microcomputed tomography (TOMCAT beamline, Swiss Light Source). Immunohistochemistry for aggrecan core protein in subsequently sectioned lung tissue demonstrated accumulation in PAH compared with failed donor lung controls. RNAscope in situ hybridization indicated *ACAN* expression in vascular endothelium and smooth muscle cells. Based on qualitative

This is an open access article under the terms of the Creative Commons Attribution-NonCommercial License, which permits use, distribution and reproduction in any medium, provided the original work is properly cited and is not used for commercial purposes.

© 2023 The Authors. *Pulmonary Circulation* published by Wiley Periodicals LLC on behalf of the Pulmonary Vascular Research Institute.

histological analysis, aggrecan localizes to cellular, rather than fibrotic or collagenous, lesions. Interestingly, *ADAMTS15*, a potential aggrecanase, was upregulated in pulmonary arteries in PAH. Aligning traditional histological analysis with three-dimensional renderings of pulmonary arteries from synchrotron imaging identified aggrecan in lumen-reducing lesions containing loose, cell-rich connective tissue, at sites of intrapulmonary bronchopulmonary shunting, and at sites of presumed elevated pulmonary blood pressure. Our findings suggest that *ACAN* expression may be an early response to injury in pulmonary angiopathy and supports recent work showing that dysregulation of aggrecan turnover is a hallmark of arterial adaptations to altered hemodynamics. Whether cause or effect, aggrecan and aggrecanase regulation in PAH are potential therapeutic targets.

#### KEYWORDS

extracellular matrix, proteoglycan, pulmonary arterial hypertension, synchrotron imaging, vascular disease

## INTRODUCTION

Endothelial injury, followed by vascular smooth muscle cell (vSMC) hypertrophy, hyperplasia, and migration, as well as excessive extracellular matrix (ECM) deposition, are thought to underlie the development of pulmonary angiopathy seen in pulmonary arterial hypertension (PAH).<sup>1,2</sup> ECM expansion and remodeling start in all three layers of the pulmonary vascular wall at early stages following vascular injury, before the onset of medial hypertrophy and elevation of pulmonary artery pressure.<sup>3,4</sup> Despite recent therapeutic advances, irreversible vascular remodeling eventually develops and is associated with high morbidity and mortality.

ECM proteoglycans, composed of core proteins to which glycosaminoglycan (GAG) chains are covalently attached, are abundant in the setting of systemic vascular injury and are facilitators of phenotype modulation, proliferation, and migration of vSMCs through cell-ECM interactions.<sup>5</sup> However, to what extent accumulation of individual proteoglycans contributes to the histopathological changes in PAH is unknown. Proteoglycans have inherent osmotic properties, determined by the number of negative charges on the GAG chains. Thus, GAG-rich proteoglycans, such as the chondroitin-sulfate (CS) and keratan-sulfate (KS) proteoglycans versican and aggrecan, can produce significant Donnan swelling pressure in tissue. This property is exemplified by the high aggrecan levels in cartilage, a tissue that has evolved to be compression-resistant.<sup>6,7</sup> In the context of the vasculature, the osmotic and biomechanical properties of aggrecan can contribute on the one hand to a

functionally-vital characteristic of umbilical arteries which facilitates their closure at birth,<sup>8</sup> and on the other hand to disruption of vessel wall integrity and development of thoracic aortic aneurysms and dissections.<sup>9</sup> Previous studies have also found aggrecan accumulation in veins grafted to a high-pressure environment, implying aggrecan production as an adaptive mechanism for altered pressures.<sup>10</sup> Versican, which is highly homologous to aggrecan, albeit with only 10% of its GAG chains, has been shown to be upregulated in vascular lesions of human idiopathic PAH (IPAH).<sup>11</sup> Several proteoglycans, including aggrecan, were also shown to be upregulated in a real-time PCR analysis of pulmonary arteries from IPAH patients.<sup>12</sup> However, the spatial distribution of aggrecan, whether it accumulates in pulmonary angiopathy of IPAH, and the mechanisms of its presence and turnover, remain to be determined.

Pre-capillary connections between the bronchial and pulmonary circulation have been identified in the setting of elevated pulmonary arterial pressure.<sup>13,14</sup> Such intrapulmonary bronchopulmonary anastomoses are linked to shunting of blood from the pulmonary to the systemic circulation in IPAH.<sup>15</sup> The pathology of PAH has been challenging to determine using conventional two-dimensional histological techniques, because of the complex vascular anatomy and branching patterns of the lung.<sup>16</sup> Therefore, there is a need for three-dimensional high-resolution imaging modalities to better understand the architecture of diseased pulmonary vasculature. Several methods for micrometer-resolution imaging of the lung were previously utilized,<sup>17,18</sup> but synchrotron radiation microcomputed tomography (SR $\mu$ CT), which

allows for superior fine detail discrimination in biological tissue with low and homogenous X-ray absorption properties was used only recently.<sup>16</sup> The highly coherent X-rays generated by the synchrotron enable the use of phase contrast, in addition to attenuation, to visualize micro-scale structures within soft tissues of the lung. Using this technique, we previously identified and described four distinct types of plexiform lesions, the histopathological hallmark lesions of PAH.<sup>19</sup> The present study aimed to investigate the accumulation and spatial distribution of aggrecan in patients with IPAH, combining traditional histological techniques with SR $\mu$ CT.

## METHODS

### Tissue and clinical data collection

Archived paraffin-embedded lung tissue from 11 patients with IPAH, collected between the years 2002 and 2014, was obtained from the pathology biobank at Skåne University Hospital, Lund, Sweden. IPAH was diagnosed according to international standards<sup>20</sup> and advanced IPAH was defined as a Heath and Edwards grade  $> 3$ .<sup>21</sup> Suprasystemic mean pulmonary arterial pressure (mPAP) was defined as  $mPAP > \text{mean arterial pressure (MAP)}$  at the time of catheterization in the individual patient. Tissue from five failed lung donors (FLD), rejected for transplant use, provided by coauthor Prof. Gunilla Westergren-Thorsson at Lund University were used as controls. Clinical data were extracted from medical records. Tissue for gene expression analysis and PCR experiments in pulmonary arteries was obtained from a separate cohort of IPAH patients and downsized donor lung controls, as previously described.<sup>22,23</sup> The study was approved by the Swedish regional ethical committee (Dnr. 2017/597 and Dnr. 2019-01769).

### SR $\mu$ CT

A full workflow of SR $\mu$ CT imaging in correlation to histology is shown in Figure 1. Imaging of IPAH paraffin-embedded tissue blocks (Figure 1a–c) was performed as previously described<sup>16,19</sup> at the X02DA TOMCAT beamline, Swiss Light Source (SLS), at the Paul Scherrer Institute (Villigen, Switzerland). Differentiation between pulmonary arteries and pulmonary veins was confirmed by comparing Elastica van Gieson (EvG) staining from serially sectioned tissue blocks (Figure 1d) with their corresponding

synchrotron images (Figure 1e). For insight into data processing and three-dimensional reconstructions, please see Supporting Information S1.

### Histology, immunohistochemistry, and immunofluorescence

Following image acquisition at the synchrotron, paraffin-embedded lung tissue from IPAH patients and FLD controls was sectioned at 4 or 5  $\mu\text{m}$  thickness. Alcian Blue/Periodic Acid Schiff (Ab/PAS) and EvG stainings were performed according to standard protocols for clinical samples at the Department of Pathology, Skåne University Hospital, Lund. For Ab/PAS staining, 1% Alcian Blue Solution (pH 2.7) and 1% Periodic Acid were used.

Aggrecan stainings used for quantification were repeated on three separate occasions for all IPAH and FLD patients. Please see Supplemental information I2 for immunohistochemistry and immunofluorescence protocols and Table ST1 for primary and secondary antibody specifications. Histological slides were digitized using the Aperio ScanScope digital slide scanner (Leica Microsystems). Images and scale bar references were captured in the Aperio ImageScope 12.4 (Leica Biosystems) software, and the Positive Pixel Count version 9 tool (Table ST2) in this software was used to quantify DAB-positive staining.

### Combined RNA in situ hybridization and immunofluorescent staining

In situ hybridization (ISH) for human *ACAN* (506841; Advanced Cell Diagnostics) followed by immunofluorescence for  $\alpha$ -smooth muscle actin (SMA), von Willebrand Factor (vWF) and Claudin 5 was performed using RNAscope (Advanced Cell Diagnostics) as described previously<sup>26</sup> (Table ST1). Fluorescent images were captured using a Zeiss AxioPhot 2 Fluorescent Microscope with a Hamamatsu C4742-95 camera and a X-cite series 120Q lamp (Lumen Dynamics) and processed in the Openlab 5 software (Improvision).

### Gene expression analysis in small pulmonary arteries

Quantitative polymerase chain reaction (qPCR) was performed on RNA extracted from laser capture microdissected small pulmonary arteries from downsized donor lungs ( $n = 8$ ) and IPAH patients ( $n = 13$ ) as

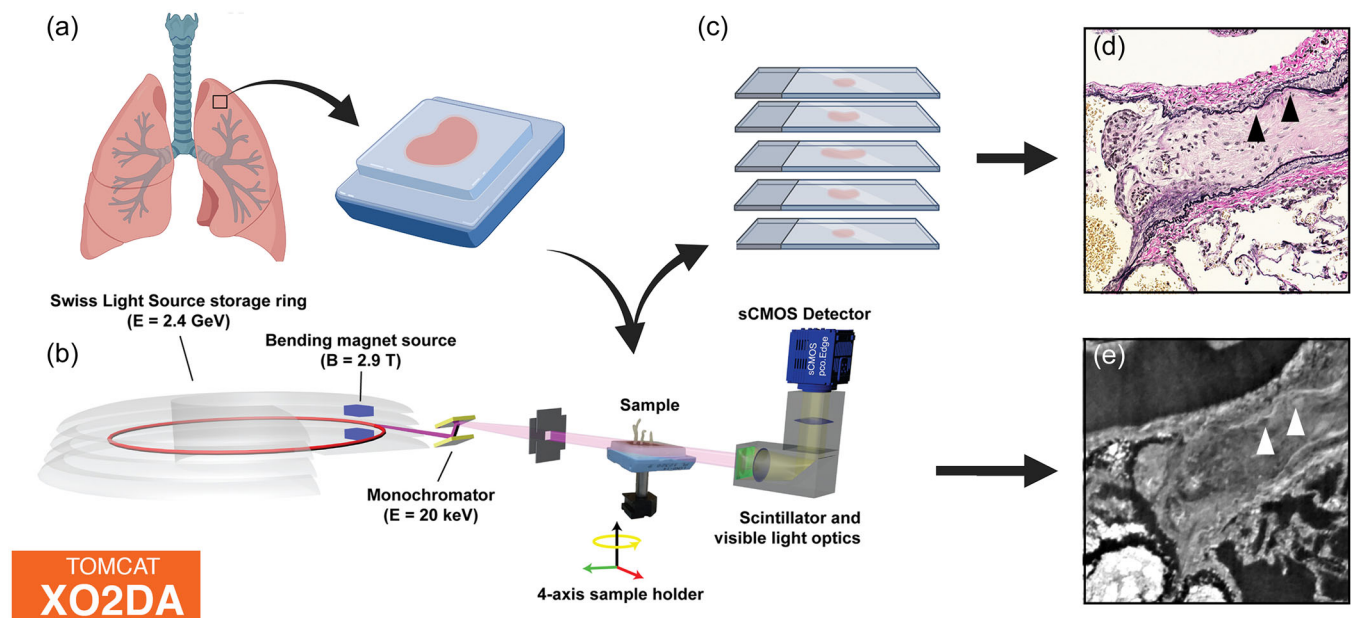


**FIGURE 1** Schematic workflow of the experimental design, including synchrotron-imaging at the X02DA TOMCAT beamline, Swiss Light Source. Paraffin-embedded lung tissue from patients with idiopathic pulmonary arterial hypertension (a) underwent synchrotron-based phase contrast microcomputed tomography (b). Synchrotron radiation was produced by a 2.9 T bending magnet inserted on the 2.4 GeV storage ring. The x-ray beam was led through a monochromator and tuned to 20 keV. The paraffin block samples were placed on a moving stage, which enabled alignment and rotation during a tomographic scan. A detecting system, comprising a scintillator and an optical microscope coupled to a sCMOS detector, was then used to collect images. Upon passing through the biological samples, mounted on sample holders using beeswax, the x-rays undergo phase-shift: variations in density within the sample parenchyma generates differences in phase-shift and subsequently image contrast. Wax markers were used to indicate areas of interest on the paraffin block samples, selected from hematoxylin staining, with or without eosin counterstaining, performed before imaging. Areas with evident air pockets were avoided, since air trapped during embedding produces significant artefacts. Experimental parameters were adjusted to image  $4.2 \times 4.2 \times 3.5$  mm volumes with an effective voxel size of  $1.63 \times 1.63 \times 1.63$   $\mu\text{m}$ , with an approximate acquisition time of 2.4 min per tomographic scan. To use propagation-based phase-contrast, the sample to detector distance was set to 19 cm. The algorithm of Paganin et al<sup>24</sup> and the gridrec algorithm<sup>25</sup> were used for phase retrieval and tomographic reconstruction, respectively. Each scanned volume was saved as a volumetric data set composed of 2160 image sections at 16-bit pixel depth. Schematics of the TOMCAT beamline are re-published with the authors permission.<sup>16</sup> Tissue blocks underwent subsequent serial sectioning and staining (c). Synchrotron-based phase-contrast micro-CT enabled identification of large structures in the pulmonary parenchyma, as well as the distinction of individual layers of the arterial wall, as confirmed by EvG staining (d and e). The internal and external elastic laminae were readily distinguishable in the synchrotron images (d) and (e) black and white arrowheads). B, magnetic field; E, energy; GeV, giga-electronvolt; keV, kilo-electronvolt; sCMOS, scientific Complementary Metal-Oxide-Semiconductor; T, Tesla.

previously described.<sup>12,22</sup> Small pulmonary arteries were defined by an intima-media diameter of 50–500  $\mu\text{m}$ . Patient characteristics were reported previously.<sup>12,27</sup> RNA was prepared for qPCR as previously described.<sup>22</sup> Primer sequences can be found in Table ST3.

## Statistical analysis

All graphs and statistical analysis were generated using GraphPad Prism version 8 (GraphPad Software). For parametric continuous variables, a Student two-tailed *t*-test was applied. For non-parametric

continuous variables, the Mann–Whitney *U* test was applied. *p*-values  $\leq 0.05$  were considered significant.

## RESULTS

### Clinical characteristics of IPAH and FLD patients

Clinical parameters of IPAH and FLD patients are outlined in Table 1. FLD patients were significantly older than IPAH patients (median 57 vs. 35 years,  $p = 0.0144$ ). All patients in the diseased group met IPAH



**TABLE 1** Clinical characteristics of IPAH and FLD controls.

	IPAH (n = 11)	FLD (n = 5)
Sex, M/F	2/9	3/2
Age at diagnosis, years	27 (23–48) <sup>a</sup>	-
Disease duration, years	2 (1–7) <sup>a</sup>	-
<b>LTX</b>		
Age at LTX*, years	35 (24–49) <sup>a</sup>	57 (52–64) <sup>a</sup>
BMI at LTX, kg/m <sup>2</sup>	23.2 (20.5–24.2) <sup>a</sup>	-
WHO functional class at LTX		
II, n (%)	0 (0%)	-
III, n (%)	5 (54.5%)	-
IV, n (%)	6 (45.5%)	-
6MWT before LTX, m	280 (100–380) <sup>a</sup>	-
<b>Medication</b>		
ERA + PDE5i, n (%)	1 (9.1%)	-
ERA + PGI <sub>2</sub> , n (%)	4 (36.4%)	-
ERA + PDE5i + PGI <sub>2</sub> , n (%)	6 (54.5%)	-
<b>Hemodynamics before LTX</b>		
SaO <sub>2</sub> , %	93 (89–96) <sup>a</sup>	-
Hb, g/L	140 (132–154) <sup>a</sup>	-
mAP, mmHg <sup>†</sup>	84 (77–92) <sup>a</sup>	-
mPAP, mmHg	68 (60–80) <sup>a</sup>	-
PVR, iWU <sup>†</sup>	15.5 (11.8–24.9) <sup>a</sup>	-
Suprasystemic mPAP, n (%)	6 (54.5%)	-
SV, mL <sup>†</sup>	40 (33.3–49.6) <sup>a</sup>	-

Note: Disease duration was defined as the time from diagnosis until tissue sampling. Suprasystemic mPAP was defined as mPAP > mAP during cardiac catheterization.

Abbreviations: BMI, body mass index; ERA, Endothelin receptor antagonist; FLD, Failed lung donor; Hb, hemoglobin; IPAH, Idiopathic pulmonary arterial hypertension; LTX, lung transplantation; mAP, mean arterial pressure; mPAP, mean pulmonary arterial pressure; PDE5i, phosphodiesterase type 5 inhibitor; PGI<sub>2</sub>, prostaglandin I<sub>2</sub>/prostacyclin; PVR, pulmonary vascular resistance; 6MWT, non-encouraged 6-minute walk test; SaO<sub>2</sub>, arterial oxygen saturation; SV, stroke volume; WHO, World Health Organization.

<sup>a</sup>Median with interquartile range.

\*Statistically significant difference, Mann–Whitney *U* test, *p* ≤ 0.05.

<sup>†</sup>*n* = 10.

diagnostic criteria and all but one patient suffered from advanced IPAH. All biopsies from IPAH patients were taken from explanted recipient lungs following lung transplantation. One individual underwent single lung transplantation, and all the other patients underwent double lung transplantation. One IPAH patient suffered from diabetes mellitus, one had systemic hypertension

and one was treated for hypothyroidism. FLD patients did not have any known pulmonary diseases.

## Variations in extracellular matrix composition in IPAH vascular lesions

As outlined by Heath and Edwards, the intimal reaction between the morphological stages two and six of PAH can be distinguished by EvG staining.<sup>21</sup> The cellular intimal reaction is characteristic of early stage vascular lesion formation. As IPAH advances, intimal lesions become collagenous (reddish pink in EvG) and eventually fibroelastic at even later stages (black in EvG). To investigate the distribution of aggrecan in IPAH lesions, four patients with IPAH were selected for complete serial sectioning and subsequent serial staining to aid in the identification and differentiation of different vascular matrices (Figure 2a–c). Staining with alcian blue (Ab) showed that acid mucins were more abundant in cellular vascular matrices, than in fibroelastic or collagenous vascular matrices (Figure 2e–g). Aggrecan accumulated in lesions composed of cellular connective tissue, rather than collagenous or fibroelastic vascular matrices (Figure 2i–k) and colocalized with Ab staining as it is a sulfated glycosaminoglycan (Figure 2e,i,h,l). Cellular and collagenous/fibroelastic matrices could often be found in close proximity with each other at branching points or within vascular lesions (Figure 2d,h,l).

## Aggrecan accumulation in IPAH vascular lesions

Immunohistochemistry demonstrated accumulation of aggrecan in multiple vascular lesion types of IPAH (Figures 2i–k and 3). Strong staining for aggrecan was observed in hypertrophic tunica media, intimal thickening, and plexiform lesions in all 11 IPAH patients (Figure 3a). In contrast, little or no aggrecan was seen in healthy arterioles and muscular arteries in FLD controls (Figure 3b), with the exception of rarely found stained areas at sites of bifurcations (Figure 3b, bottom panel). Negative and positive controls are provided for comparison (Figure 3c,d). Quantification of aggrecan staining revealed that IPAH patients displayed a statistically significant increase in strongly stained (*p* = 0.0071) and total stained (*p* = 0.0068) positive pixels per section, compared to controls (Figure 3e). No aggrecan accumulation was seen in pulmonary veins, airways, or pulmonary parenchyma of IPAH lungs, however aggrecan was present in large elastic arteries of both IPAH and FLD patients (Figure S1). Immunofluorescent stainings

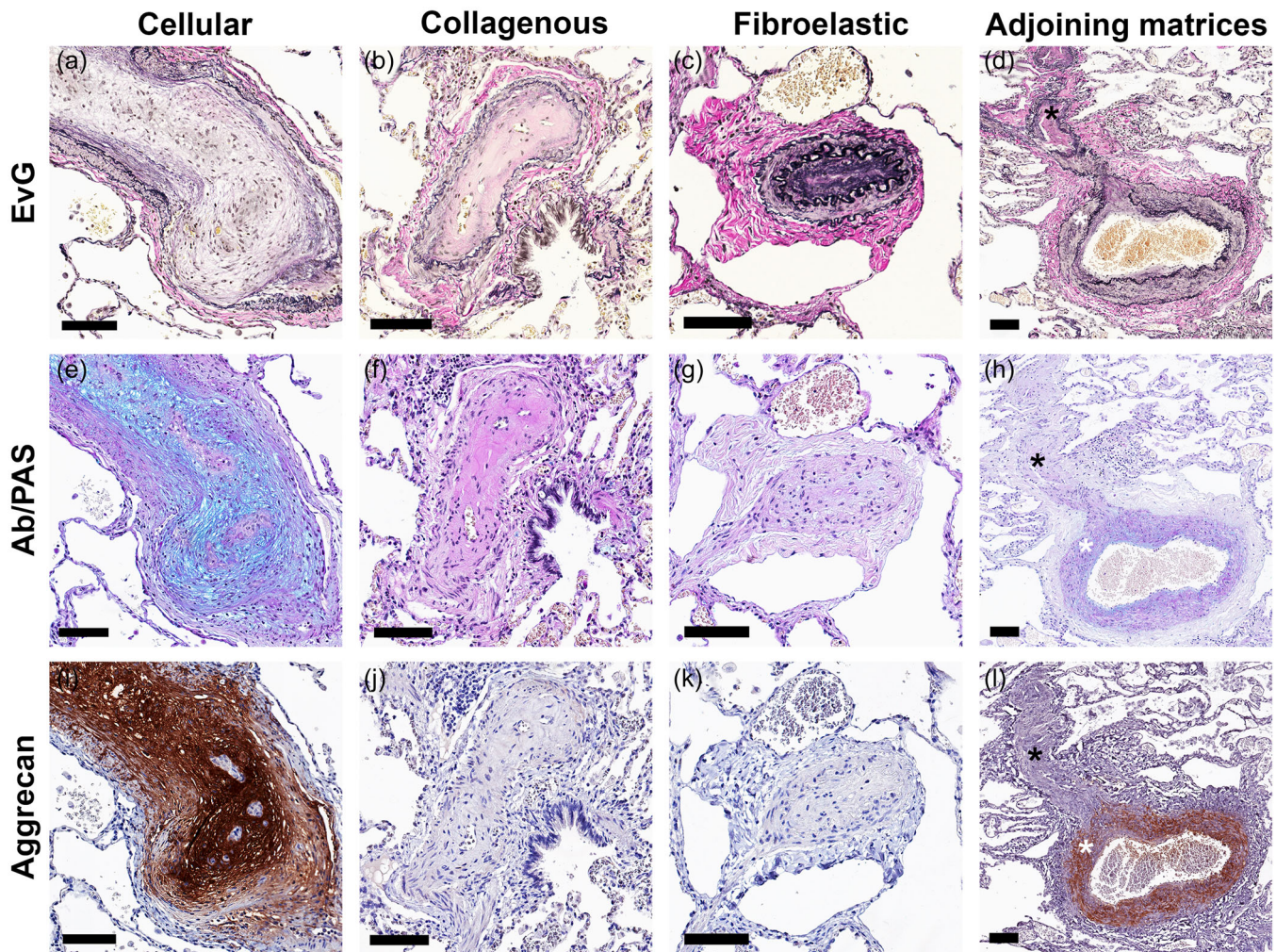


**FIGURE 2** Diversity of extracellular matrix composition in IPAH vascular lesions. Serial sectioning and histological staining allowed for differentiation of vascular matrices in IPAH. EvG stainings suggested the existence of cellular (a), collagenous (b) and fibroelastic (c) matrices in intimal lesions, medial hypertrophy and plexiform lesions. Cellular matrices contained minimal collagen (reddish pink) and elastin (black). In contrast, collagenous matrices and fibroelastic matrices stained strongly for collagen or a combination of collagen and elastin. Ab/PAS identified acidic mucins (blue), neutral mucins (magenta) and mixtures of the two (purple). Cellular connective tissue matrices accumulated acidic mucins (e), whereas collagenous (f) and fibroelastic (g) matrices did not. When performing subsequent immunohistochemistry for aggrecan, only cellular connective tissue matrix lesions exhibited notable aggrecan staining (i–k). Occluded distal arterioles could display a collagenous or fibroelastic matrix composition (d, black asterisk) with negative mucin (h, black asterisk) and aggrecan (l, black asterisk) staining, whereas the hypertrophic parent muscular artery was rich in cellular connective tissue (d, white asterisk), acidic mucins (h, white asterisk) and aggrecan (l, white asterisk). Representative images are shown. All scale bars measure 200  $\mu\text{m}$ . Ab/PAS, Alcian blue/Periodic Acid Schiff; EvG, Elastica van Gieson.

for aggrecan and versican revealed that both proteoglycans were found in diseased vessels, colocalizing in medial hypertrophy but to a lesser extent in intimal hyperplasia and plexiform lesions (Figure S2).

### Local production of ACAN mRNA in vascular lesions of IPAH

Combined RNAscope ISH and immunofluorescence were performed to identify *ACAN*-expressing cells in IPAH lesions

(Figure 4). *ACAN* ISH demonstrated expression in medial hypertrophy (Figure 4a,b), intimal lesions (Figure 4e,f) and plexiform lesions (Figure 4i,j) of IPAH. Combined *ACAN* RNAscope with SMA immunofluorescence revealed that regions positive for SMA also contained *ACAN* mRNA in medial hypertrophy (Figure 4c,d). Possible co-localization of *ACAN* mRNA and cell regions positive for vWF was seen in intimal (Figure 4g,h) and plexiform lesions (Figure 4k,l) and a similar pattern was seen when staining for the alternative endothelial marker Claudin 5 (Figure S3). Cells expressing *ACAN* that appeared to be negative for all markers tested,



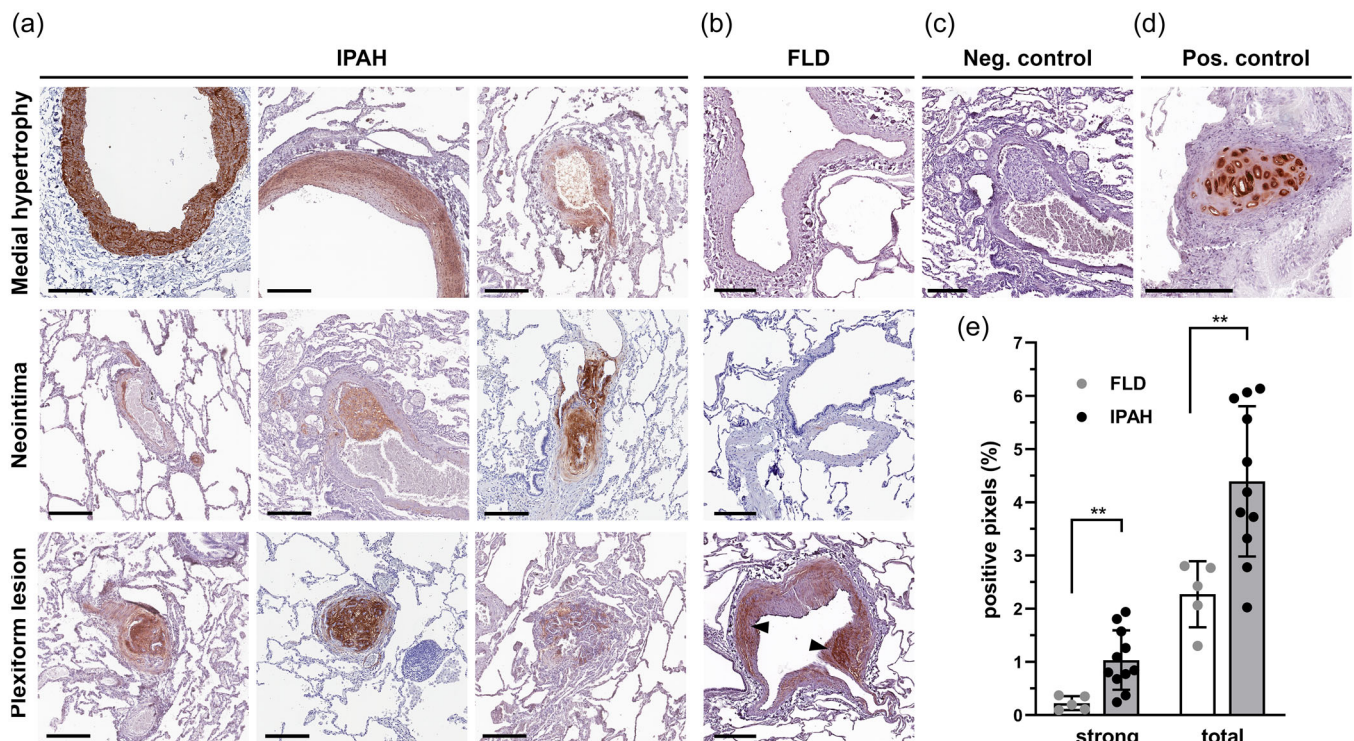


**FIGURE 3** Aggrecan accumulates in multiple types of IPAH vascular lesions. Representative images of aggrecan immunohistochemistry demonstrated accumulation in hypertrophic media, intimal lesions, and plexiform lesions of all 11 IPAH patient samples (a). FLD control pulmonary arteries generally demonstrated little or no staining for aggrecan, however, some aggrecan was seen at branching sites in some sections (b, black arrowheads). Representative images are shown from nine IPAH patients and three FLD patients (a and b). Negative control (c) and airway cartilage positive control (d) are shown for comparison. All scale bars measure 200  $\mu\text{m}$ . Quantifying and comparing aggrecan stainings between IPAH and FLD patients revealed a significantly higher percentage of strong and total pixel positivity in IPAH patients compared to controls (e). Data are plotted as mean  $\pm$  SD. Each datapoint represents an average of measurements from three individually performed stainings.  $**p \leq 0.01$ . FLD, failed lung donor; IPAH, idiopathic pulmonary arterial hypertension.

however, were also observed and remain to be identified (Figure 4c,d,g,h,k,l).

### Increased ACAN and ADAMTS15 expression in IPAH pulmonary arteries

Presence of *ACAN* has been reported previously in small and large pulmonary arteries of IPAH patients<sup>12</sup> with increased accumulation in large arteries. However, little is known about the *ACAN* degrading enzymes in IPAH. Therefore, mRNA expression analysis was performed for genes encoding proteoglycan-degrading enzymes *ADAMTS1*, *ADAMTS4*, *ADAMTS5*, *ADAMTS9*, *ADAMTS15*, *ADAMTS20*, *MMP3*, and *MMP13* in small pulmonary arteries. Gene expression levels for *ADAMTS4*, *ADAMTS20*, *MMP3*, and *MMP13* were below the mRNA detection limit, and these were therefore excluded from further analysis. No significant differences between IPAH and donor pulmonary arteries were detected for *ADAMTS1*, *ADAMTS5*, and *ADAMTS9* (Figure 5a–c), but

a trend towards higher protease expression in IPAH was observed. Significantly higher expression of *ADAMTS15* ( $p = 0.0124$ ) was, however, found in small IPAH pulmonary arteries compared to controls (Figure 5d).

### Accumulation of aggrecan at sites of intrapulmonary bronchopulmonary shunting

Segmentation and three-dimensional rendering, combined with multiple virtual sectioning planes of IPAH lesions allowed a better analysis of aggrecan localization within the pulmonary vascular tree in three patients with IPAH (Figure 6). Patient 1 displayed specific aggrecan staining in a pulmonary artery with hypertrophic tunica media and within an intimal occlusion of the same vessel, but no positive aggrecan staining was seen distal to the complete occlusion or in dilated distal collaterals (Figure 6a–d). A connection between the pulmonary artery, distal to the occlusion, and the bronchial



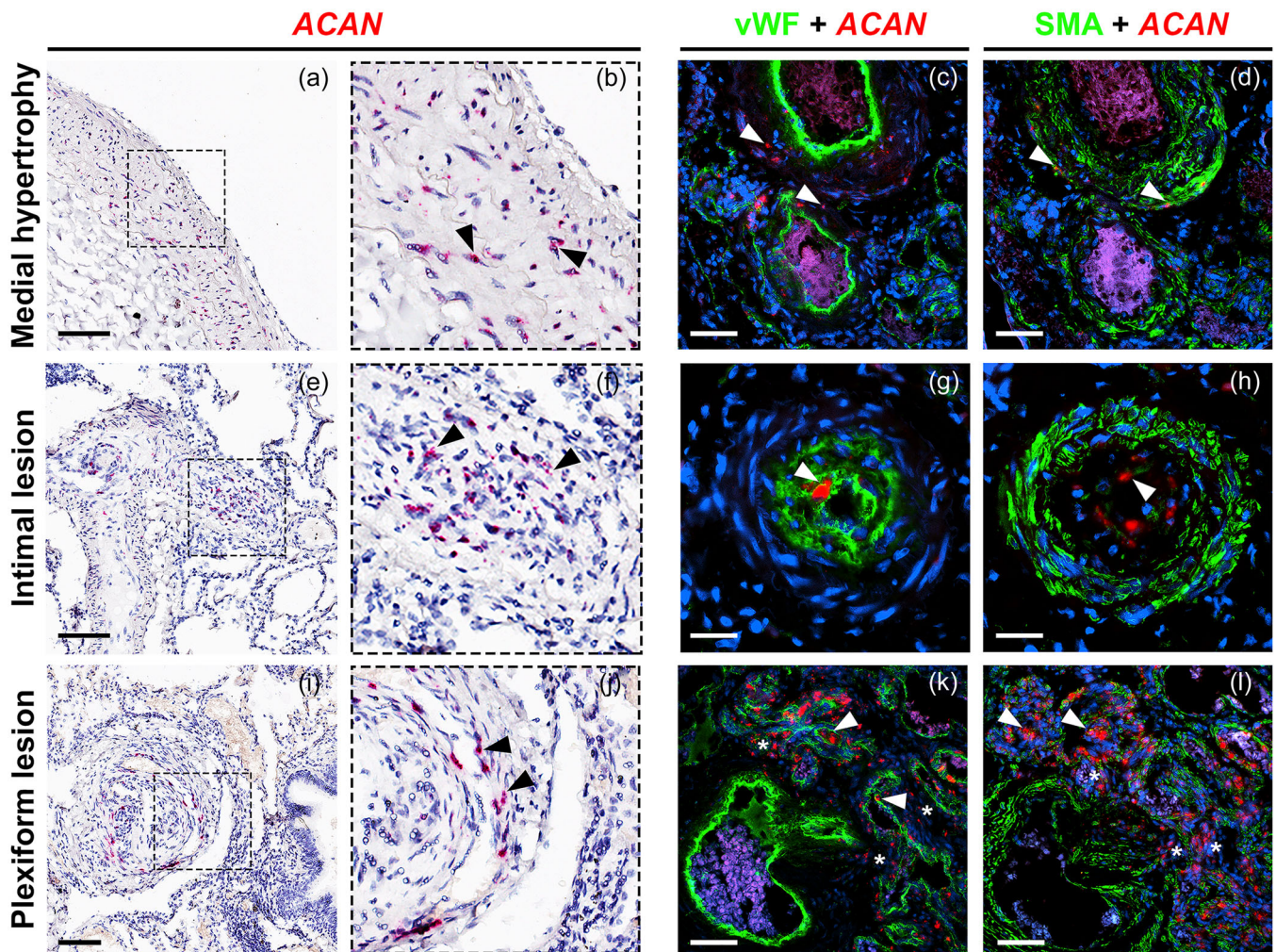


**FIGURE 4** ACAN is expressed in IPAH vascular lesions and co-localizes with regions positive for vWF and SMA. RNAscope ISH demonstrated expression of ACAN mRNA (red) in diseased vessels of IPAH patients. ACAN mRNA expression was observed in medial hypertrophy (a and b), intimal lesions (e and f, here cut lengthwise), and plexiform lesions (i and j) of IPAH patients. Combining immunofluorescence for vWF (green in c, g, k) and SMA (green in d, h, l) with ACAN ISH (red) demonstrated that SMA-positive regions, but not vWF-positive regions, expressed ACAN mRNA in medial hypertrophy (c and d, white arrowheads). In contrast, SMA-positive regions did not seem to express ACAN mRNA in intimal or plexiform lesions (h, l, white arrowheads), whereas vWF-positive regions did (g, k, white arrowheads). ACAN was also produced by cells negative for both SMA and vWF, mainly observed in plexiform lesions (k and l, white asterisks). All scale bars measure 100  $\mu\text{m}$ . ACAN, aggrecan-encoding gene; IPAH, idiopathic pulmonary arterial hypertension; mRNA, messenger RNA; vWF, von Willebrand Factor; SMA, actin  $\alpha$ -smooth muscle.

circulation of the adjacent bronchiole was also observed in Patient 1 (B, yellow arrowhead). In Patient 2, an aggrecan-rich type 4 plexiform lesion (pulmonary artery with re-canalization as previously described<sup>19</sup>) was accompanied by distal dilatation of the pulmonary artery branches, that displayed no positive aggrecan staining (Figure 6e–h). In addition, a collateral vessel connecting the pulmonary artery proximal and distal to the plexiform lesion, was apparent (Figure 6f, yellow arrowhead). Finally, in Patient 3, a type 1 plexiform lesion (within a supernumerary artery, as previously described<sup>19</sup>) exited from a hypertrophied pulmonary artery, both staining positive for aggrecan (Figure 6i–l).

Distal to the plexiform lesion, the pulmonary artery was completely occluded by a fibrotic matrix and lacked aggrecan staining. Analysis of vascular connections from the plexiform lesion showed collaterals to the vasa vasorum of the distally occluded PA (Figure 6j, yellow arrowhead). Subsequent EvG staining allowed for comparisons between matrices proximal and distal to high-pressure points and plexiform lesions in IPAH patients (Figure S4). The qualitative analysis of this data suggests an accumulation of aggrecan proximal to, as well as in lesions associated with increased mean pulmonary arterial blood pressure, whereas no accumulation was seen distal to such lesions.



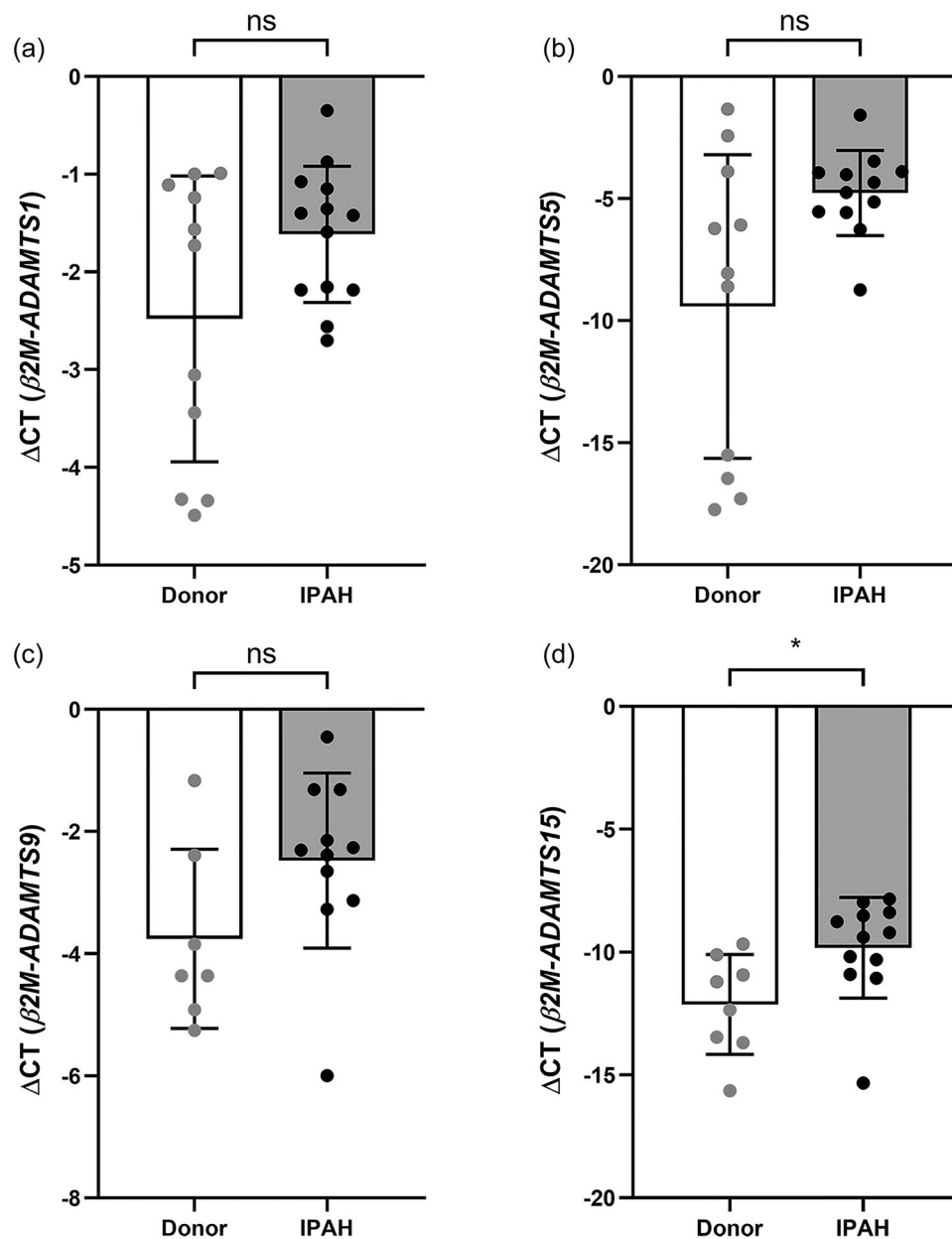


**FIGURE 5** Increased expression of *ADAMTS15* mRNA in IPAH pulmonary arteries. No significant differences were observed for expression of *ADAMTS1* (a), *ADAMTS5* (b) and *ADAMTS9* (c) in small pulmonary arteries, even though upwards trends were observed. *ADAMTS15* was however significantly upregulated in small pulmonary arteries of IPAH patients (d). Data are plotted as mean  $\pm$  SD. Each datapoint represents a single individual, with pooled mRNA from 100 vessels per individual. \* $p \leq 0.05$ . IPAH, idiopathic pulmonary arterial hypertension; mRNA, messenger RNA.

## DISCUSSION

ECM remodeling has been suggested to play key roles in development of pulmonary angiopathy in PAH.<sup>2,28</sup> Matrix composition and proteoglycan content varies with the different stages of vascular disease, as previously shown in atherosclerotic plaques.<sup>29</sup> In the systemic circulation, proteoglycans appear predominantly in early stages of vascular lesion formation, whereas fibrillar collagens and

elastic fibers increase as the vascular lesion becomes more advanced and fibrotic.<sup>5</sup> Indeed, in 1958 Heath and Edwards demonstrated a distinction between cellular and fibroelastic/collagenous intimal lesions in PAH secondary to congenital heart defects, determined by EvG staining.<sup>21</sup> Our current data allowed for a similar differentiation between cellular and collagenous/fibrotic intimal vascular lesion matrices in IPAH. Aggrecan was observed to accumulate in cellular vascular matrices in IPAH patients,

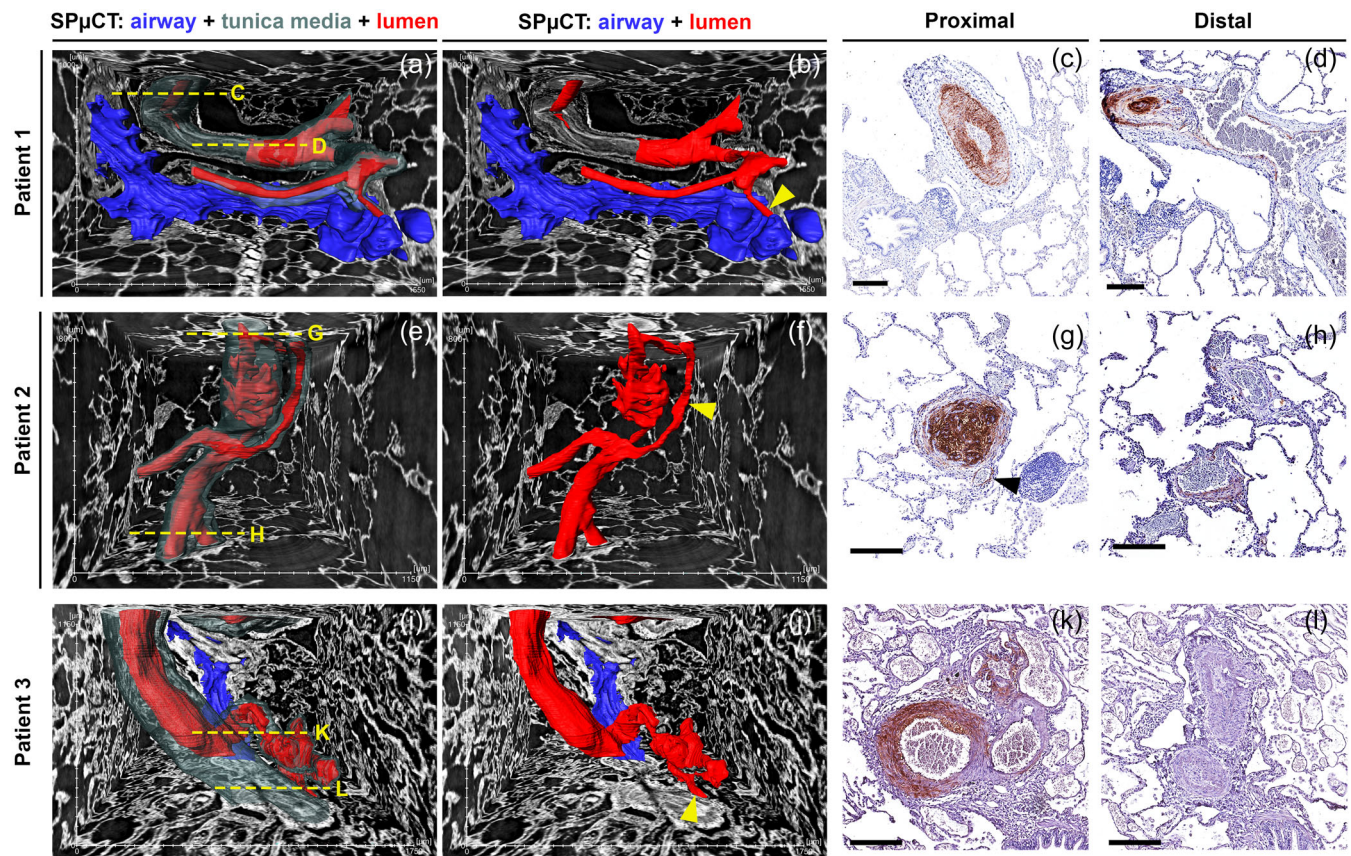


**FIGURE 6** Aggrecan preferably accumulates at high-pressure areas in IPAH. Manual and automated reconstructions of pulmonary and bronchial arteries, together with large airways, revealed positive aggrecan immunostaining at sites of increased pulmonary artery pressure in three patients with IPAH (a–l). Patient 1 (a and b) displayed specific aggrecan-positive staining within the hypertrophic media proximal to an obstructive intimal lesion, which also stained positive for aggrecan (c). No positive staining was seen distal to the occlusion (d). A small vessel connecting to the bronchial circulation of an adjacent airway was identified and rendered (b, yellow arrowhead). In Patient 2 (e and f), an aggrecan-rich type 4 plexiform lesion (g) caused narrowing of the lumen, with no positive aggrecan staining distally (h). In addition, a small shunt vessel bypassing the potential lumen-narrowing lesion is shown (f, yellow arrowhead). Patient 3 (i and j) displays a hypertrophic vessel, from which a type 1 plexiform lesion arises, both rich in aggrecan (k). Distally, the vessel is completely occluded, although lacking aggrecan staining (l). A small vessel leaving the plexiform lesion connects distally to the vasa vasorum of the distally occluded pulmonary artery (j, yellow arrowhead). IPAH, idiopathic pulmonary arterial hypertension.

but not in lesions with fibrotic or collagenous matrices. In both fibrosis and wound healing, extensively studied by Wight and co-workers,<sup>30</sup> a proteoglycan-rich “provisional matrix”, induced by hampered cell signaling or tissue injury, was shown to enable migration, signaling and differentiation of both resident and invading cells during the early repair process. Accumulation of large aggrecan-hyaluronic acid complexes supports a matrix capable of sequestering numerous GAG-binding growth factors.<sup>31,32</sup> Indeed, many factors previously shown to be of importance in pulmonary hypertension (BMPs, Wnt ligands, TGF- $\beta$ , IL-6, FGF-2, PDGF-BB, and VEGF), are GAG/heparin-binding, suggesting a role for proteoglycans in their regulation.<sup>28,33</sup> A highly hydrated matrix furthermore provides the extracellular space necessary for subsequent cell expansion and continued matrix

deposition/remodeling. As pulmonary vascular lesions age they appear to become increasingly fibro-collagenous, with proteoglycan content apparently decreasing. Viewing aggrecan as a part of the early response-to-injury, it could be a potentiator of cell migration and proliferation, in addition to contributing to luminal narrowing through the generation of a hydrated, tissue growth factor-binding matrix, but also through its ability to bind water and produce a significant osmotic swelling pressure.

Recent publications have emphasized the biomechanical importance of large aggregating proteoglycans in arterial wall homeostasis and proposed that overexpression of GAGs/proteoglycans can disrupt normal mechanosensing and may compromise vascular wall integrity.<sup>34,35</sup> Upon grafting veins to the arterial circulation in mice, proteomics revealed that aggrecan was significantly upregulated in



response to the high-pressure environment.<sup>10</sup> Furthermore, in umbilical arteries from multiple mammalian species, the inner tunica media contained abundant aggrecan compared to the outer tunica media and the venous tunica media and was computationally predicted to increase internal tunica media swelling that enabled umbilical artery closure at birth.<sup>8</sup> Here, aggrecan accumulation was seen in diseased pulmonary muscular arteries and arterioles, but not in any significant amount in FLD controls with presumed normal pulmonary pressures. Furthermore, no aggrecan accumulation was seen in veins of IPAH patients. Small aggregates of aggrecan were observed at sites of mild intimal thickening in small pulmonary vessels of the FLD controls. However, those vessels can be considered healthy as intimal fibrosis of this type is a normal finding in lungs beyond adolescence.<sup>21</sup> Perhaps supporting this notion, FLD donors were significantly older than the IPAH patients in our cohort. Although virtually impossible to obtain, an age-matched control group would have been optimal for the comparisons performed in this study, and would have removed the confounder of older controls in our data set. The presence and function of aggrecan in large elastic arteries has been touched upon by others,<sup>9,34,35</sup> and we confirm that it is present in pulmonary elastic arteries in both IPAH and FLD patients. Differential accumulation of aggrecan in IPAH could be due to differential degradation. This is supported by trends of increases in *ADAMTS1*, *ADAMTS5*, and *ADAMTS9* gene expression in small pulmonary vessels of IPAH. We also found *ADAMTS15* to be significantly upregulated in these vessels. Information on *ADAMTS15* is scarce and although observations supporting its ability to cleave versican<sup>36</sup> and recombinant aggrecan<sup>37,38</sup> were previously published, it is not considered a prominent aggrecanase in the present literature. A recent study by Santamaria et al<sup>39</sup> investigated the substrates of *ADAMTS8*, a protease whose gene locus is tightly linked with that of *ADAMTS15*, suggesting a close relationship between these proteases. Targeted deletion of *Adamts8* in myocytes and vSMCs of pulmonary arteries in mice has been associated with reduced right ventricular hypertrophy and systolic pressure, compared to wild type controls, when subjected to hypoxia-induced PAH.<sup>40</sup> Although concluded to be an inefficient aggrecanase, *ADAMTS8* cleaves osteopontin,<sup>39</sup> a phosphoprotein that is increased in plasma of patients with PAH and that correlates with disease severity and mortality.<sup>41</sup>

Combining RNAscope in situ hybridization for *ACAN* with immunofluorescence revealed that aggrecan in hypertrophic tunica media was locally produced in the lesion, mainly by what we suggest are vSMCs, and in intimal lesions and plexiform lesions, primarily in regions positive for vWF or Claudin 5. Being a secreted endothelial glycoprotein, vWF accumulation in the matrix surrounding non-endothelial cells might provide

a false positive endothelium staining, a reason why vWF staining needs to be interpreted with caution.<sup>42</sup> However, Claudin 5 staining confirmed the observed pattern. A subset of currently unidentified cells appeared to produce aggrecan in plexiform lesions. We and others have previously shown that leukocytes, determined by CD45 staining, mainly accumulate in the adventitial layer, or as leukocytic caps surrounding human plexiform lesions.<sup>11</sup> Previous work has supported the possibility that vSMCs can transdifferentiate into chondrogenic cell phenotypes in response to vascular injury,<sup>43</sup> as known producers of aggrecan. vSMCs are highly mechanosensitive and increased proteoglycan production is a known consequence of increased cyclic mechanical stress in vSMCs.<sup>44–46</sup> Together, these notions make the hypothesis of shear-stress-induced trans-differentiation of vSMCs into a chondrocyte-like phenotype in plexiform lesions tempting and motivate further studies.

Three-dimensional mapping of hypertensive lesions in IPAH, and the connections between aggrecan-rich lesions and lesions lacking aggrecan, was made possible by combining SR $\mu$ CT with traditional histology. As suggested by our group and others, certain plexiform lesions are anastomosing structures allowing for shunting of blood between the pulmonary and bronchial circulation in PAH, possibly relieving pressure from the pulmonary circulation.<sup>15,16,19</sup> Here, aggrecan was observed to accumulate in hypertrophic tunica media proximal to such pressure-relieving plexiform lesions in IPAH patients. Aggrecan accumulation was also witnessed in supernumerary arteries entering plexiform lesions, in addition to its presence within the plexiform lesion itself. However, in dilated collaterals exiting plexiform lesions, where pulmonary pressure is believed to be low, no aggrecan was observed. Whether aggrecan is the cause or effect of an elevated pulmonary arterial pressure in plexiform lesions and hypertrophic tunica media of IPAH cannot be concluded from this study, however, aggrecan regulation in pulmonary vSMCs and its relation to shear stress and variations in blood pressure are interesting subjects for future animal and three dimensional in vitro modeling studies of PAH.

The present study has limitations. Hypertensive diseases of the pulmonary circulation, IPAH in particular, are rare conditions and access to human tissue samples is limited.<sup>47</sup> Tissue for this study was gathered and processed over several years. Stereology and unbiased sampling was therefore not possible, limiting the possibilities of certain gold-standard quantitative measurements.<sup>48</sup> Temporal aspects of IPAH angiopathy related to aggrecan accumulation were not possible to study in this material, as all samples were taken from terminally ill patients with advanced disease. However, since a wide array of late and early stage lesions are present

in end-stage PAH,<sup>21</sup> the distinction between cellular and fibrotic/collagenous matrix types was possible in our material. Just recently, we presented promising data indicating that prolongation of the Sugen5416/Hypoxia rat model<sup>49</sup> generated the same four types of plexiform lesions previously identified in human IPAH.<sup>50</sup> Hopefully, this model will enable accurate basic temporal studies of the development of pulmonary vascular lesions.

GAGs associated with aggrecan (CS and KS) were not stained for in this study, as these are also associated with other proteoglycans located in the pulmonary vasculature of IPAH.<sup>11</sup> We provide indirect evidence of GAG accumulation in vascular lesions of IPAH, by demonstrating colocalized accumulation of acidic mucins, through alcian blue staining, and aggrecan core protein in vascular lesions of IPAH. We furthermore acknowledge the limitation that different IPAH patient groups were used for imaging combined with subsequent histology ( $n = 11$ ) and for gene expression analysis in laser capture micro-dissected small pulmonary arteries (control  $n = 8$ , IPAH  $n = 13$ ).

SR $\mu$ CT enables non-destructive visualization of biological tissues.<sup>51</sup> Its use in studies of cardiopulmonary shunts was published recently and the full potential of the method has yet to be explored.<sup>16,52</sup> As an example, standardized algorithms for measurements of disease burden in volumetric datasets of PAH are currently under development by our group, since manual reconstruction of the pulmonary microvasculature, as applied in this study, is subject to interobserver variation.

To summarize, aggrecan was expressed and deposited selectively in all types of vascular lesions of IPAH; intimal lesions, medial hypertrophy, and plexiform lesions. Qualitative analysis of synchrotron data and histological stainings suggested preferable accumulation of aggrecan just proximal to, or at high-pressure points in the pulmonary circulation, as well as in early vascular intimal matrices. Analogous with the findings in systemic<sup>5</sup> and umbilical arteries,<sup>8</sup> we speculate that the swelling resulting from the abundant GAG chains in aggrecan may have a role in arterial luminal narrowing and fibrosis development in IPAH. This could indeed be the cause of increased pulmonary arterial pressure, due to the development of intimal occlusions and type 4 plexiform lesions.<sup>19</sup> Alternatively, or additionally, aggrecan expression could be an arterial adaptive response to increased pulmonary artery pressure. Although aggrecanases were only briefly addressed in this work, we believe that mapping of degradomes related to upregulated ADAMTS enzymes in PAH may hold the key to developing therapies to halt the development of pulmonary angiopathy in its early stages, thus avoiding irreversible vascular fibrosis and remodeling.

## AUTHOR CONTRIBUTIONS

All authors made substantial contributions to conception and design, acquisition of data, or analysis and interpretation of data. Oscar van der Have and Karin Tran-Lundmark drafted the manuscript. All authors edited, revised, and approved the final version of the manuscript. Preliminary data has previously been published as an abstract: *Circulation*. 2021;144:A13141.

## ACKNOWLEDGMENTS

We acknowledge the Paul Scherrer Institute, Villigen, Switzerland, for provision of synchrotron radiation beamtime at the X02DA TOMCAT beamline of the Swiss Light Source and thank Dr. Goran Lovric and Dr. Anne Bonnin for excellent technical assistance. We also thank Mrs. Elna Lampe for excellent technical assistance. Schematic figures were created with [BioRender.com](https://BioRender.com).

## CONFLICT OF INTEREST STATEMENT

The author declare no conflict of interest.

## DATA AVAILABILITY STATEMENT

All supplemental data is available via: <https://figshare.com/s/e3857cc42d0235986866>.

## ETHICS STATEMENT

The study was approved by the Swedish regional ethical committee (Dnr. 2017/597 and Dnr. 2019-01769).

## ORCID

Oscar van der Have  <http://orcid.org/0000-0003-4726-0697>

Timothy J. Mead  <http://orcid.org/0000-0003-1891-3652>

## REFERENCES

1. Pietra GG, Capron F, Stewart S, Leone O, Humbert M, Robbins IM, Reid LM, Tuder RM. Pathologic assessment of vasculopathies in pulmonary hypertension. *JACC*. 2004;43(12 Suppl S):S25–32.
2. Thenappan T, Chan SY, Weir EK. Role of extracellular matrix in the pathogenesis of pulmonary arterial hypertension. *Am J Physiol-Heart Circ Physiol*. 2018;315(5):H1322–31.
3. Todorovich-Hunter L, Dodo H, Ye C, McCready L, Keeley FW, Rabinovitch M. Increased pulmonary artery elastolytic activity in adult rats with monocrotaline-induced progressive hypertensive pulmonary vascular disease compared with infant rats with nonprogressive disease. *Am Rev Respir Dis*. 1992;146(1):213–23.
4. Tuder RM. Pulmonary vascular remodeling in pulmonary hypertension. *Cell Tissue Res*. 2017;367(3):643–49.
5. Wight TN. A role for proteoglycans in vascular disease. *Matrix Biol*. 2018;71–72:396–420.
6. Kiani C, Chen L, Wu YJ, Yee AJ, Yang BB. Structure and function of aggrecan. *Cell Res*. 2002;12(1):19–32.



7. Chandran PL, Horkay F. Aggrecan, an unusual poly-electrolyte: review of solution behavior and physiological implications. *Acta Biomater.* 2012;8(1):3–12.
8. Nandadasa S, Szafron JM, Pathak V, Murtada SI, Kraft CM, O'Donnell A, Norvik C, Hughes C, Caterson B, Domowicz MS, Schwartz NB, Tran-Lundmark K, Veigl M, Sedwick D, Philipson EH, Humphrey JD, Apte SS. Vascular dimorphism ensured by regulated proteoglycan dynamics favors rapid umbilical artery closure at birth. *eLife.* 2020;9:e60683.
9. Cikach FS, Koch CD, Mead TJ, Galatioto J, Willard BB, Emerton KB, Eagleton MJ, Blackstone EH, Ramirez F, Roselli EE, Apte SS. Massive aggrecan and versican accumulation in thoracic aortic aneurysm and dissection. *JCI Insight.* 2018;3(5):e97167.
10. Suna G, Wojakowski W, Lynch M, Barallobre-Barreiro J, Yin X, Mayr U, Baig F, Lu R, Fava M, Hayward R, Molenaar C, White SJ, Roleder T, Milewski KP, Gasior P, Buszman PP, Buszman P, Jahangiri M, Shanahan CM, Hill J, Mayr M. Extracellular matrix proteomics reveals interplay of aggrecan and aggrecanases in vascular remodeling of stented coronary arteries. *Circulation.* 2018;137(2):166–83.
11. Chang YT, Chan CK, Eriksson I, Johnson PY, Cao X, Westöö C, Norvik C, Andersson-Sjöland A, Westergren-Thorsson G, Johansson S, Hedin U, Kjellén L, Wight TN, Tran-Lundmark K. Versican accumulates in vascular lesions in pulmonary arterial hypertension. *Pulm Circ.* 2016;6(3):347–59.
12. Jandl K, Marsh LM, Hoffmann J, Mutgan AC, Baum O, Bloch W, Thekkekara-Puthenparampil H, Kolb D, Sinn K, Klepetko W, Heinemann A, Olschewski A, Olschewski H, Kwapiszewska G. Basement membrane remodeling controls endothelial function in idiopathic pulmonary arterial hypertension. *Am J Respir Cell Mol Biol.* 2020;63(1):104–17.
13. Humbert M, Guignabert C, Bonnet S, Dorfmueller P, Klinger JR, Nicolls MR, Olschewski AJ, Pullamsetti SS, Schermuly RT, Stenmark KR, Rabinovitch M. Pathology and pathobiology of pulmonary hypertension: state of the art and research perspectives. *Eur Respir J.* 2019;53(1):1801887.
14. Turner-Warwick M. Precapillary systemic-pulmonary anastomoses. *Thorax.* 1963;18:225–37.
15. Galambos C, Sims-Lucas S, Abman SH, Cool CD. Intrapulmonary bronchopulmonary anastomoses and plexiform lesions in idiopathic pulmonary arterial hypertension. *Am J Respir Crit Care Med.* 2016;193(5):574–76.
16. Norvik C, Westöö CK, Peruzzi N, Lovric G, van der Have O, Mokso R, Jeremiasen I, Brunnström H, Galambos C, Bech M, Tran-Lundmark K. Synchrotron-based phase-contrast micro-CT as a tool for understanding pulmonary vascular pathobiology and the 3-D microanatomy of alveolar capillary dysplasia. *Am J Physiol-Lung Cell Mol Physiol.* 2020;318(1):L65–75.
17. Scott AE, Vasilescu DM, Seal KAD, Keyes SD, Mavrogordato MN, Hogg JC, Sinclair I, Warner JA, Hackett TL, Lackie PM. Three dimensional imaging of paraffin embedded human lung tissue samples by micro-computed tomography. *PLoS One.* 2015;10(6):e0126230.
18. Clark DP, Badaea CT. Micro-CT of rodents: state-of-the-art and future perspectives. *Phys Med.* 2014;30(6):619–34.
19. Westöö C, Norvik C, Peruzzi N, van der Have O, Lovric G, Jeremiasen I, Tran PK, Mokso R, de Jesus Perez V, Brunnström H, Bech M, Galambos C, Tran-Lundmark K. Distinct types of plexiform lesions identified by synchrotron-based phase-contrast micro-CT. *Am J Physiol-Lung Cell Mol Physiol.* 2021;321(1):L17–28.
20. Simonneau G, Montani D, Celermajer DS, Denton CP, Gatzoulis MA, Krowka M, Williams PG, Souza R. Haemodynamic definitions and updated clinical classification of pulmonary hypertension. *Eur Respir J.* 2019;53(1):1801913.
21. Heath D, Edwards JE. The pathology of hypertensive pulmonary vascular disease; a description of six grades of structural changes in the pulmonary arteries with special reference to congenital cardiac septal defects. *Circulation.* 1958;18(4 Part 1):533–47.
22. Hoffmann J, Wilhelm J, Marsh LM, Ghanim B, Klepetko W, Kovacs G, Olschewski H, Olschewski A, Kwapiszewska G. Distinct differences in gene expression patterns in pulmonary arteries of patients with chronic obstructive pulmonary disease and idiopathic pulmonary fibrosis with pulmonary hypertension. *Am J Respir Crit Care Med.* 2014;190(1):98–111.
23. Hoffmann J, Wilhelm J, Olschewski A, Kwapiszewska G. Microarray analysis in pulmonary hypertension. *Eur Respir J.* 2016;48(1):229–41.
24. Paganin D, Mayo SC, Gureyev TE, Miller PR, Wilkins SW. Simultaneous phase and amplitude extraction from a single defocused image of a homogeneous object. *J Microsc.* 2002;206(Pt 1):33–40.
25. Marone F, Stampanoni M. Re-gridding reconstruction algorithm for real-time tomographic imaging. *J Synchrotron Radiat.* 2012;19(Pt 6):1029–37.
26. Mead TJ, Apte SS. Expression analysis by RNAscope in situ hybridization. *Methods Mol Biol.* 2020;2043:173–78.
27. Hoffmann J, Marsh LM, Pieper M, Stacher E, Ghanim B, Kovacs G, König P, Wilkens H, Haïtchi HM, Hoefler G, Klepetko W, Olschewski H, Olschewski A, Kwapiszewska G. Compartment-specific expression of collagens and their processing enzymes in intrapulmonary arteries of IPAH patients. *Am J Physiol-Lung Cell Mol Physiol.* 2015;308(10):L1002–13.
28. Tannenbergs P, Tran-Lundmark K. The extracellular matrix in early and advanced pulmonary arterial hypertension. *Am J Physiol-Heart Circ Physiol.* 2018;315(6):H1684–86.
29. Otsuka F, Kramer MCA, Woudstra P, Yahagi K, Ladich E, Finn AV, de Winter RJ, Kolodgie FD, Wight TN, Davis HR, Joner M, Virmani R. Natural progression of atherosclerosis from pathologic intimal thickening to late fibroatheroma in human coronary arteries: a pathology study. *Atherosclerosis.* 2015;241(2):772–82.
30. Wight TN, Potter-Perigo S. The extracellular matrix: an active or passive player in fibrosis? *Am J Physiol-Gastrointest Liver Physiol.* 2011;301(6):G950–55.
31. Tannenbergs P, Chang YT, Muhl L, Laviña B, Gladh H, Genové G, Betsholtz C, Folestad E, Tran-Lundmark K. Extracellular retention of PDGF-B directs vascular remodeling in mouse hypoxia-induced pulmonary hypertension. *Am J Physiol-Lung Cell Mol Physiol.* 2018;314(4):L593–L605.
32. Sheikh AQ, Misra A, Rosas IO, Adams RH, Greif DM. Smooth muscle cell progenitors are primed to muscularize in pulmonary hypertension. *Sci Transl Med.* 2015;7(308):308ra159.
33. Kjellén L, Lindahl U. Proteoglycans: structures and interactions. *Annu Rev Biochem.* 1991;60:443–75.

34. Roccabianca S, Ateshian GA, Humphrey JD. Biomechanical roles of medial pooling of glycosaminoglycans in thoracic aortic dissection. *Biomech Model Mechanobiol*. 2014;13(1):13–25.
35. Roccabianca S, Bellini C, Humphrey JD. Computational modelling suggests good, bad and ugly roles of glycosaminoglycans in arterial wall mechanics and mechanobiology. *J R Soc Interface*. 2014;11(97):20140397.
36. Stupka N, Kintakas C, White JD, Fraser FW, Hanciu M, Aramaki-Hattori N, Martin S, Coles C, Collier F, Ward AC, Apte SS, McCulloch DR. Versican processing by a disintegrin-like and metalloproteinase domain with thrombospondin-1 repeats proteinases-5 and -15 facilitates myoblast fusion. *J Biol Chem*. 2013;288(3):1907–17.
37. Porter S, Clark IM, Kevorkian L, Edwards DR. The ADAMTS metalloproteinases. *Biochem J*. 2005;386(Pt 1):15–27.
38. Guo C, Tsigkou A, Lee MH. ADAMTS13 and 15 are not regulated by the full length and N-terminal domain forms of TIMP-1, -2, -3 and -4. *Biomed Rep*. 2016;4(1):73–8.
39. Santamaria S, Martin DR, Dong X, Yamamoto K, Apte SS, Ahnström J. Post-translational regulation and proteolytic activity of the metalloproteinase ADAMTS8. *J Biol Chem*. 2021;297(5):101323.
40. Omura J, Satoh K, Kikuchi N, Satoh T, Kurosawa R, Nogi M, Ohtsuki T, Al-Mamun ME, Siddique MAH, Yaoita N, Sunamura S, Miyata S, Hoshikawa Y, Okada Y, Shimokawa H. ADAMTS8 promotes the development of pulmonary arterial hypertension and right ventricular failure: a possible novel therapeutic target. *Circ Res*. 2019;125(10):884–906.
41. Mura M, Cecchini MJ, Joseph M, Granton JT. Osteopontin lung gene expression is a marker of disease severity in pulmonary arterial hypertension. *Respirology*. 2019;24(11):1104–10.
42. Steffes LC, Cheng P, Quertermous T, Kumar ME. von Willebrand factor is produced exclusively by endothelium, not neointima, in occlusive vascular lesions in both pulmonary hypertension and atherosclerosis. *Circulation*. 2022;146(5):429–31.
43. Speer MY, Yang HY, Brabb T, Leaf E, Look A, Lin WL, Frutkin A, Dichek D, Giachelli CM. Smooth muscle cells give rise to osteochondrogenic precursors and chondrocytes in calcifying arteries. *Circ Res*. 2009;104(6):733–41.
44. Leung DYM, Glagov S, Mathews MB. Cyclic stretching stimulates synthesis of matrix components by arterial smooth muscle cells in vitro. *Science*. 1976;191(4226):475–77.
45. Li C, Xu Q. Mechanical stress-initiated signal transduction in vascular smooth muscle cells in vitro and in vivo. *Cell Signal*. 2007;19(5):881–91.
46. Lee RT, Yamamoto C, Feng Y, Potter-Perigo S, Briggs WH, Landschulz KT, Turi TG, Thompson JF, Libby P, Wight TN. Mechanical strain induces specific changes in the synthesis and organization of proteoglycans by vascular smooth muscle cells. *J Biol Chem*. 2001;276(17):13847–51.
47. Hoepfer MM, Humbert M, Souza R, Idrees M, Kawut SM, Sliwa-Hahnle K, Jing ZC, Gibbs JSR. A global view of pulmonary hypertension. *Lancet Respir Med*. 2016;4(4):306–22.
48. Ochs M, Mühlfeld C. Quantitative microscopy of the lung: a problem-based approach. Part 1: basic principles of lung stereology. *Am J Physiol-Lung Cell Mol Physiol*. 2013;305(1):L15–22.
49. Taraseviciene-Stewart L, Kasahara Y, Alger L, Hirth P, Mahon GM, Waltenberger J, Voelkel NF, Tudor RM. Inhibition of the VEGF receptor 2 combined with chronic hypoxia causes cell death-dependent pulmonary endothelial cell proliferation and severe pulmonary hypertension. *FASEB J*. 2001;15(2):427–38.
50. van der Have O, Westoo C, Ahrne F, Tian X, Ichimura K, Dreier T, Norvik C, Kumar ME, Spiekerkoetter E, Tran-Lundmark K. Shunt-type plexiform lesions identified in the Sugen5416/Hypoxia rat model of pulmonary arterial hypertension using SPmicroCT. *Eur Respir J*. 2022;59(6):2102802.
51. Momose A, Takeda T, Itai Y, Hirano K. Phase-contrast x-ray computed tomography for observing biological soft tissues. *Nature Med*. 1996;2(4):473–75.
52. Iwaki R, Matsuhisa H, Hoshino M, Oshima Y. Three-dimensional evaluation of ductal tissue in coarctation of the aorta using x-ray phase-contrast tomography. *J Thorac Cardiovasc Surg*. 2016;152(5):1454–56.

## SUPPORTING INFORMATION

Additional supporting information can be found online in the Supporting Information section at the end of this article.

**How to cite this article:** van der Have O, Mead TJ, Westöö C, Peruzzi N, Mutgan AC, Norvik C, Bech M, Struglics A, Hoetzenecker K, Brunnström H, Westergren-Thorsson G, Kwapiszewska G, Apte SS, Tran-Lundmark K. Aggrecan accumulates at sites of increased pulmonary arterial pressure in idiopathic pulmonary arterial hypertension. *Pulm Circ*. 2023;13:e12200.  
<https://doi.org/10.1002/pul2.12200>